Comprehensive search for buckled honeycomb binary compounds based on noble metals (Cu, Ag, and Au)

Shota Ono [*]

Department of Electrical, Electronic and Computer Engineering, Gifu University, Gifu 501-1193, Japan

Honeycomb structure has frequently been observed in two-dimensional (2D) materials. CuAu in the buckled honeycomb (BHC) structure was synthesized recently, which is a case of a 2D intermetallic compound. Here, the dynamical stability of 2D AX in the BHC structure, where $A = $ Cu, Ag, and Au, and X is a metallic element in the Periodic Table, is systematically studied by calculating phonon dispersions from first-principles. Among 135 AX, 48 AX are identified to be dynamically stable. In addition, we discuss (i) the relationship between the dynamical stability and the formation energy, (ii) a correlation of the dynamical stability between different constituents A, and (iii) trends of the structural, elastic, electronic, and magnetic properties. Furthermore, a stable phase of the B11-type AuZr is predicted based on both the result (ii) and the stability relationship between 2D and 3D structures. The stability of B11 AuZr is consistent with other predictions using the machine learning approach. The present findings should stimulate future studies exploring the physics and chemistry of 2D intermetallic compounds.

I. INTRODUCTION

The two-dimensional (2D) compound of CuAu has been synthesized experimentally [1], and the CuAu system has a buckled honeycomb (BHC) structure that is the same as the stable structure of silicene and germanene. This discovery opens the way for studying 2D compounds including only metallic elements. The fundamental properties of 2D elemental metals, such as energetic, structural, and elastic properties [2,3], dynamical stability [4,5], and magnetic properties [6], have been investigated systematically from first-principles, also motivated by recent experimental synthesis of 2D metals [7–11]. It is desirable to extend such investigations for 2D intermetallic compounds that are difficult to find (currently) in 2D materials databases [12–16].

Copper, silver, and gold belong to the noble metal column in the Periodic Table, so the effects of d electrons on their electronic and optical properties have been studied extensively under various conditions [17–20]. For the compounds including noble metals, it is not trivial to understand their stability properties among CuX, AgX, and AuX, where X is an element in the Periodic Table, as confirmed by, for example, Pettifor's structure map [21] or a modern materials database [22]. Recently, Alsalmi *et al.* have studied the stability of CuZn, AgZn, and AuZn in the B2 (CsCl-type) structure by using density functional theory (DFT) [23], and they explained the nonmonotonic behaviors of structural parameters, where AgZn takes the largest lattice constant. This is never achieved by studying each compound individually. A systematic investigation for the stability of 2D CuX, AgX, and AuX will thus be of fundamental importance.

In a previous paper, the author studied a stability relationship between 2D and 3D Cu-based compounds and found that if a CuX (X is a metallic element) in the BHC structure is dynamically stable, that in the B_h (WC-type) and $L1_1$ (CuPt-type) structures is also dynamically stable [24]. This is due to the geometric hierarchy: B_h ($L1_1$) structure can be constructed from ABAB (ABC) stacking of hexagonal layers of Cu and X alternately. In addition, it has been shown that an experimental synthesis of the B_h structure accounts for the dynamical stability of the BHC structure; for example, LiRh, LiPd, LiIr, and LiPt [25]. In this way, the BHC structure can serve as a building block for constructing 3D compounds.

In this paper, we present systematic investigations of the dynamical stability for the BHC CuX, AgX, and AuX, where X is a metallic element from Li to Pb in the Periodic Table, by using a first-principles approach. We identify that 48 compounds are dynamically stable by quantifying the profile of the phonon spectra. We demonstrate that the quantity for the dynamical stability of AgX is correlated with that of AuX. Based on this fact, we predict that as a 3D compound, AuZr in the B11 (CuTi-type) structure is dynamically stable, which is consistent with other predictions based on the machine learning approach [26]. Trends of the structural parameters, formation energy, elastic constants, electronic bands, and magnetic property are also discussed. We identify that the BHC AXs ($A = $ Cu,Ag,Au; $X = $ K,Rb,Cs) are wide-gap semiconductors, and that the BHC AgCr, AuCr, CuMn, AgMn, and AuMn have a magnetic moment about $4\mu_B$ with a Bohr magneton μ_B. The calculated results are listed in Table I including the values of the modified formation energy defined in Eq. (1) and the degree of the dynamical stability defined in Eq. (2); in Table II including the lattice parameters of the BHC CuX, AgX, and AuX; and in Table III including

———————
[*]shota_o@gifu-u.ac.jp

TABLE I. The values of E_{form} in units of eV (columns 2, 3, and 4) and S (columns 5, 6, and 7) for BHC AX. The value of S is shown in bold if $S \geqslant 0.6$.

| | A | | | A | | |
X	Cu	Ag	Au	Cu	Ag	Au
Li	−0.47	−0.64	−0.83	**1.00**	**0.82**	**0.98**
Na	0.40	−0.12	−0.19	−2.03	−0.53	0.91
K	0.71	0.01	−0.57	−2.22	−1.17	**1.00**
Rb	0.70	−0.00	−0.61	−2.75	−1.05	−1.11
Cs	0.65	−0.11	−0.71	−1.25	−2.54	−0.67
Be	−0.42	0.35	0.25	**0.97**	−3.86	−2.63
Mg	−0.24	−0.56	−0.66	−0.21	**0.89**	**0.97**
Ca	0.02	−0.40	−0.97	−3.01	−2.03	−1.51
Sr	0.19	−0.25	−0.90	−4.53	−3.28	−2.01
Ba	0.12	−0.28	−1.00	−3.57	−4.00	−1.64
Sc	−0.84	−1.01	−1.39	−2.19	**1.00**	**0.66**
Y	−0.70	−0.95	−1.47	−3.94	−1.19	−0.97
Lu	−0.89	−1.08	−1.66	−4.08	−0.86	−0.98
Ti	−1.07	−0.96	−1.13	0.01	**1.00**	**0.92**
Zr	−0.82	−0.97	−1.15	−3.05	**0.66**	**0.83**
Hf	−1.06	−1.11	−1.35	−3.13	**1.00**	**0.81**
V	−0.94	−0.43	−0.51	−4.29	−14.96	−24.01
Nb	−0.90	−0.79	−0.89	−1.60	−1.70	−1.22
Ta	−0.99	−0.84	−0.94	−3.19	−2.78	−1.76
Cr	−1.07	−0.67	−0.70	−3.47	**0.85**	**0.86**
Mo	−1.02	−0.64	−0.68	−2.97	−2.48	−2.18
W	−1.08	−0.70	−0.70	−2.31	−2.51	−3.08
Mn	−0.84	−0.72	−0.79	**1.00**	**1.00**	**0.76**
Tc	−1.07	−0.52	−0.47	−4.35	−5.01	−5.44
Re	−1.10	−0.52	−0.39	−2.26	−3.36	−3.72
Fe	−0.75	−0.22	−0.23	−2.63	−2.42	−3.12
Ru	−1.01	−0.50	−0.38	−1.28	0.12	0.55
Os	−0.99	−0.40	−0.15	−1.75	−1.36	−1.98
Co	−0.73	−0.03	0.03	**1.00**	−0.63	−0.29
Rh	−0.96	−0.60	−0.43	**0.75**	**0.83**	**0.85**
Ir	−0.90	−0.44	−0.13	−0.25	0.52	−0.77
Ni	−0.76	−0.12	−0.02	**0.91**	−0.17	−0.87
Pd	−0.89	−0.78	−0.56	**0.86**	**1.00**	**0.76**
Pt	−0.75	−0.54	−0.22	**0.79**	**0.83**	**0.97**
Cu	−0.51	−0.14	−0.09	**1.00**	**0.69**	**0.88**
Ag	−0.14	−0.33	−0.25	**0.69**	**0.75**	**0.88**
Au	−0.09	−0.25	−0.10	**0.88**	**0.88**	**0.87**
Zn	−0.41	−0.23	−0.25	**1.00**	0.50	**1.00**
Cd	0.02	−0.31	−0.30	−0.85	**0.82**	**0.93**
Hg	0.45	0.02	0.10	−3.29	−2.90	−2.18
Al	−0.72	−0.57	−0.64	**1.00**	**0.91**	**0.87**
Ga	−0.42	−0.44	−0.44	**0.65**	**0.62**	**0.83**
In	0.11	−0.29	−0.23	−3.24	−0.45	−0.85
Tl	0.42	−0.07	0.05	−5.67	−1.67	−3.17
Sn	0.07	−0.27	−0.19	−4.98	−0.62	−1.16
Pb	0.33	−0.11	0.04	−6.05	−2.44	−2.99

TABLE II. The values of $d(A\text{-}A)$ (columns 2, 3, and 4) and $d(A\text{-}X)$ (columns 5, 6, and 7) for BHC AX. The smaller value, $d(A\text{-}A)$ or $d(A\text{-}X)$, is underlined for each AX.

| | A | | | A | | |
X	Cu	Ag	Au	Cu	Ag	Au
Li	2.63	2.92	2.91	<u>2.51</u>	<u>2.68</u>	<u>2.60</u>
Na	<u>2.84</u>	<u>3.06</u>	<u>2.98</u>	2.93	3.08	2.99
K	5.55	5.69	5.56	<u>3.20</u>	<u>3.29</u>	<u>3.21</u>
Rb	5.75	5.95	5.78	<u>3.32</u>	<u>3.44</u>	<u>3.34</u>
Cs	5.94	6.23	5.98	<u>3.43</u>	<u>3.60</u>	<u>3.45</u>
Be	<u>2.39</u>	2.69	2.84	2.40	<u>2.58</u>	<u>2.38</u>
Mg	2.84	2.99	2.98	<u>2.72</u>	<u>2.92</u>	<u>2.83</u>
Ca	3.69	3.72	3.89	<u>2.87</u>	<u>3.03</u>	<u>2.88</u>
Sr	4.07	4.13	4.27	<u>3.03</u>	<u>3.19</u>	<u>3.04</u>
Ba	4.47	4.49	4.66	<u>3.14</u>	<u>3.31</u>	<u>3.17</u>
Sc	3.10	3.14	3.29	<u>2.67</u>	<u>2.90</u>	<u>2.74</u>
Y	3.44	3.43	3.64	<u>2.81</u>	<u>3.01</u>	<u>2.86</u>
Lu	3.32	3.33	3.54	<u>2.74</u>	<u>2.94</u>	<u>2.78</u>
Ti	2.71	<u>2.85</u>	2.89	<u>2.66</u>	2.90	<u>2.80</u>
Zr	2.96	<u>3.00</u>	3.07	<u>2.77</u>	3.01	<u>2.89</u>
Hf	2.97	3.01	3.09	<u>2.72</u>	<u>2.96</u>	<u>2.83</u>
V	<u>2.51</u>	<u>2.72</u>	<u>2.75</u>	2.66	2.87	2.81
Nb	<u>2.71</u>	<u>2.80</u>	<u>2.82</u>	2.77	3.00	2.95
Ta	<u>2.75</u>	<u>2.82</u>	<u>2.85</u>	2.72	2.97	2.90
Cr	<u>2.44</u>	2.88	2.87	2.60	<u>2.86</u>	<u>2.82</u>
Mo	<u>2.63</u>	<u>2.73</u>	<u>2.75</u>	2.69	2.94	2.90
W	<u>2.67</u>	<u>2.74</u>	<u>2.76</u>	2.67	2.93	2.90
Mn	2.63	<u>2.83</u>	2.84	<u>2.59</u>	2.85	<u>2.82</u>
Tc	<u>2.59</u>	<u>2.69</u>	<u>2.71</u>	2.64	2.89	2.87
Re	<u>2.61</u>	<u>2.69</u>	<u>2.71</u>	2.64	2.90	2.88
Fe	<u>2.48</u>	<u>2.70</u>	<u>2.73</u>	2.58	2.83	2.80
Ru	<u>2.58</u>	<u>2.70</u>	<u>2.72</u>	2.62	2.88	2.89
Os	<u>2.60</u>	<u>2.68</u>	<u>2.70</u>	2.63	2.91	2.91
Co	<u>2.44</u>	<u>2.67</u>	<u>2.70</u>	2.55	2.77	2.78
Rh	<u>2.60</u>	<u>2.72</u>	<u>2.73</u>	2.61	2.86	2.88
Ir	<u>2.61</u>	<u>2.69</u>	<u>2.71</u>	2.63	2.91	2.95
Ni	<u>2.45</u>	<u>2.68</u>	<u>2.71</u>	2.51	2.72	2.73
Pd	<u>2.65</u>	<u>2.78</u>	<u>2.77</u>	2.64	2.84	2.89
Pt	2.66	<u>2.75</u>	<u>2.74</u>	<u>2.66</u>	2.89	2.97
Cu	<u>2.50</u>	<u>2.73</u>	<u>2.74</u>	2.57	2.76	2.78
Ag	<u>2.73</u>	<u>2.86</u>	<u>2.82</u>	2.76	2.98	3.06
Au	<u>2.74</u>	<u>2.82</u>	<u>2.77</u>	2.78	3.06	3.30
Zn	<u>2.53</u>	<u>2.76</u>	<u>2.75</u>	2.74	2.96	2.99
Cd	<u>2.80</u>	<u>2.91</u>	<u>2.87</u>	2.91	3.15	3.18
Hg	<u>2.88</u>	<u>2.99</u>	<u>2.89</u>	2.93	3.19	3.34
Al	2.65	<u>2.81</u>	2.83	<u>2.61</u>	2.86	<u>2.82</u>
Ga	2.65	<u>2.84</u>	2.83	<u>2.68</u>	2.96	2.97
In	2.98	<u>3.06</u>	3.01	<u>2.83</u>	3.09	3.06
Tl	3.26	3.19	3.36	<u>2.84</u>	<u>3.17</u>	<u>2.98</u>
Sn	3.13	3.13	3.12	<u>2.76</u>	<u>3.05</u>	<u>2.98</u>
Pb	3.33	3.26	3.24	<u>2.80</u>	<u>3.12</u>	<u>3.05</u>

the elastic constants for the selected BHC compounds. The computational details are described in Appendix.

II. BASIC CONCEPTS

The primitive lattice vectors of the BHC structure are $\boldsymbol{a}_1 = a_{\text{lat}}(1, 0, 0)$, $\boldsymbol{a}_2 = a_{\text{lat}}(-1/2, \sqrt{3}/2, 0)$, and $\boldsymbol{a}_3 =$ $(0, 0, c)$ with the lattice constant a_{lat}. For the BHC AX with $A = $ Cu, Ag, and Au and X a metallic element, the basis vectors are $A(0, 0, \delta)$ and $X(0, a_{\text{lat}}/\sqrt{3}, -\delta)$ with the total thickness 2δ. The interatomic distance $d(A\text{-}A)$ between the same species is equal to a_{lat}, while the interatomic distance $d(A\text{-}X)$ between the atoms A and X is given by $a_{\text{lat}}\sqrt{1/3 + 4r^2}$ with $r = \delta/a_{\text{lat}}$ (see Fig. 1).

TABLE III. The values of c_{11}, c_{12}, and c_{22} (in units of GPa nm) and Δ of the selected BHC AX.

AX	c_{11}	c_{12}	c_{22}	$\log_{10} \Delta$
CuLi	39.0	23.1	40.0	3.0
AgLi	35.0	21.5	36.2	2.9
AuLi	35.9	34.8	40.4	2.4
AuNa	39.5	26.6	35.9	2.9
AuK	6.2	5.4	6.2	1.0
CuBe	115.9	32.4	115.3	4.1
AgMg	45.8	16.8	44.8	3.2
AuMg	38.7	19.9	38.5	3.0
AgSc	27.6	22.2	27.6	2.4
AuSc	23.9	10.3	24.1	2.7
CuTi	42.5	34.9	42.4	2.8
AgTi	61.8	38.0	61.9	3.4
AuTi	46.9	34.1	46.9	3.0
AgZr	50.6	30.6	50.5	3.2
AuZr	38.8	23.8	38.8	3.0
AgHf	61.0	30.3	60.9	3.4
AuHf	51.4	22.1	51.4	3.3
AgCr	56.0	9.9	58.5	3.5
AuCr	55.2	13.4	57.9	3.5
CuMn	54.9	9.0	56.0	3.5
AgMn	68.1	26.8	66.6	3.6
AuMn	70.4	32.5	63.3	3.5
CuCo	136.1	52.9	136.7	4.2
CuRh	141.8	55.9	142.0	4.2
AgRh	139.1	58.7	139.1	4.2
AuRh	155.2	73.4	155.0	4.3
CuNi	132.7	47.5	132.5	4.2
CuPd	127.3	42.9	127.5	4.2
AgPd	109.7	38.1	109.6	4.0
AuPd	132.4	55.2	132.3	4.2
CuPt	176.3	56.5	176.3	4.4
AgPt	160.4	52.5	160.6	4.4
AuPt	175.3	58.0	175.3	4.4
CuCu	99.6	37.1	102.8	3.9
AgCu	83.8	34.8	83.4	3.8
AuCu	93.6	44.9	99.2	3.9
AgAg	73.8	32.7	75.5	3.7
AgAu	105.7	43.0	102.3	4.0
AuAu	136.3	54.9	142.6	4.2
CuZn	98.0	30.6	103.1	4.0
AuZn	88.2	38.6	93.0	3.8
AgCd	67.9	24.8	71.0	3.6
AuCd	89.8	35.1	90.1	3.8
CuAl	97.5	24.1	97.2	3.9
AgAl	85.6	29.5	87.9	3.8
AuAl	82.5	43.6	85.1	3.7
CuGa	69.9	30.1	71.4	3.6
AgGa	68.4	26.9	65.9	3.6
AuGa	73.6	44.7	72.5	3.5

FIG. 1. Top and side views for the 2D AX in the BHC structure with the lattice constant a_{lat}, the thickness 2δ, and the interatomic distances $d(A\text{-}A)$, $d(A\text{-}X)$, and $d(X\text{-}X)$.

for most cases because the 2D structures are energetically unstable (but might be dynamically stable) [25]. To obtain a useful insight from the energy calculations, we define a modified formation energy as

$$E_{\mathrm{form}}(AX) = \varepsilon_{\mathrm{BHC}}(AX) - [\varepsilon_{\mathrm{HX}}(A) + \varepsilon_{\mathrm{HX}}(X)], \qquad (1)$$

where $\varepsilon_{\mathrm{BHC}}(AX)$ is the total energy of AX in the BHC structure, and $\varepsilon_{\mathrm{HX}}(A)$ is the total energy of A in the hexagonal (HX) structure. The physics behind Eq. (1) is that vertically stacking the HX layers of A and X produces the BHC structure of AX by releasing or absorbing energies: When $E_{\mathrm{form}}(AX) < 0$, BHC AX is energetically suitable to be formed from HX layers.

For the elemental metals of X, 46 elements were investigated in the present work, so that the phonon dispersions for 135 compounds were calculated. To systematically understand the dynamical stability property of AX, we define the degree of the dynamical stability as

$$S = \frac{R - (1 - p)}{p} \qquad (2)$$

with

$$R = \frac{\omega_{\max} + \mathrm{sgn}(\omega_{\min}^2)|\omega_{\min}|}{\omega_{\max}}, \qquad (3)$$

where $\omega_{\max}$ and $\omega_{\min}$ are the maximum and minimum phonon frequencies, respectively, which are calculated by the phonon density-of-states (DOS). An imaginary frequency is represented as a negative frequency by using the sign function of sgn. If no imaginary frequency is observed in the phonon DOS, $R = 1$ exactly, otherwise $R < 1$. Due to a finite size of the q grid in the Brillouin zone, small imaginary frequencies may appear around the Γ point. To identify an unstable structure clearly, we subtract $1 - p$ from R and normalize the value by dividing p. In the present work, we adapted the value of $p = 0.1$. The negative (or small positive) value of S indicates an instability of AX in the BHC structure.

The elastic properties have been studied in a variety of 2D materials, allowing us to understand the relationship with the structural properties [2,13,14,27]. For the 48 compounds having $0.6 \leqslant S \leqslant 1$ and the CuTi ($S = 0.01$), we calculated the elastic constants, c_{11}, c_{12}, and c_{22}, for the in-plane deformations. The c_{ij}'s ($i, j = 1, 2$) are related to the potential energy defined as

$$E_{\mathrm{strain}}(AX) = \tfrac{1}{2} c_{11} \varepsilon_x^2 + c_{12} \varepsilon_x \varepsilon_y + \tfrac{1}{2} c_{22} \varepsilon_y^2, \qquad (4)$$

The formation energy is usually defined as the energy difference between the total energy of the binary system considered (such as ordered compounds and/or alloys) and that of the reference system (ground-state structure of elements, such as fcc, bcc, and hcp). Application of this standard formula to 2D binary compounds yielded positive formation energies
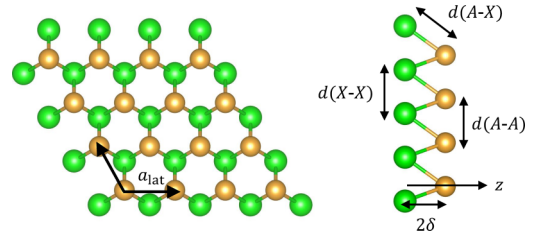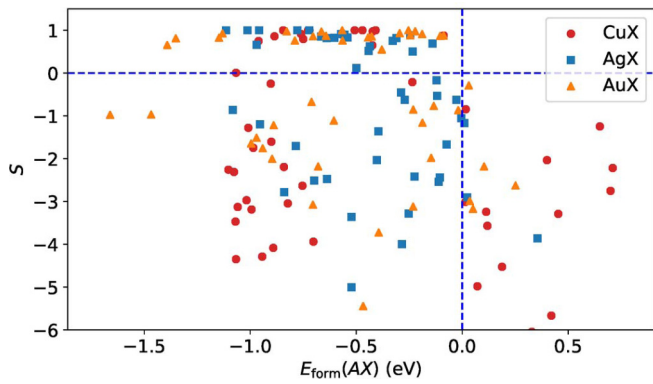
FIG. 2. Plot of S as a function of E_{form} for the BHC CuX, AgX, and AuX. Dashed lines indicate $E_{\text{form}} = 0$ (vertical) and $S = 0$ (horizontal).

where ε_x and ε_y are the strain along the x and y directions [2]. The determinant of the Hessian matrix of E_{strain} is given by

$$\Delta(AX) = c_{11}c_{22} - c_{12}^2. \tag{5}$$

If $\Delta(AX) > 0$, the AX in the BHC structure is elastically stable, that is, the BHC AX is stable against the long-wavelength phonons in the longitudinal and transverse acoustic branches.

III. RESULTS AND DISCUSSION

A. Dynamical stability

Table I lists the values of $E_{\text{form}}(AX)$ in Eq. (1) and S in Eq. (2) for CuX, AgX, and AuX in the BHC structure. The values of S are distributed from -6 (unstable) to 1 (stable), except for AgV and AuV. The BHC AX having a relatively high value of S will be a cousin of 2D CuAu [1], which will expand the family of 2D intermetallic compounds. The calculated phonon dispersions for CuX, AgX, and AuX are provided in the Supplemental Material [28].

We first study a correlation between $E_{\text{form}}(AX)$ and S. As shown in Fig. 2, the AX having positive S shows negative $E_{\text{form}}(AX)$, indicating that the formation energy modified to treat an energy gain for stacking HX layers [see Eq. (1)] may be a good quantity for studying the dynamical stability of AX. This improves our previous results [25], where the 2D compound that is dynamically stable can have a positive formation energy (even in the BHC CuAu compounds) when

the standard formation energy is applied. However, the negative value of $E_{\text{form}}(AX)$ is still not a sufficient condition for yielding the positive S. The negative S implies a structure transformation from the BHC to more complex geometry.

Note that we have also studied the formation energy with respect to the energies of the isolated atoms, i.e., $E_{\text{form}}^{\text{atom}}(AX) = \varepsilon_{\text{BHC}}(AX) - [\varepsilon_{\text{atom}}(A) + \varepsilon_{\text{atom}}(X)]$, where $\varepsilon_{\text{atom}}(X)$ is the energy of a single atom X in a supercell. A similar definition of $E_{\text{form}}^{\text{atom}}(AX)$ has been used to study the stability of the honeycomb structures of group-IV elements and III-V binary compounds [27]. The $E_{\text{form}}^{\text{atom}}(AX)$ dependence of S is qualitatively the same as that depicted in Fig. 2: the compounds having positive S show negative $E_{\text{form}}^{\text{atom}}(AX)$. However, only five compounds of CuK (0.01 eV), CuRb (0.08 eV), CuCs (0.10 eV), CuHg (0.36 eV), and AuHg (0.01 eV) have been identified to be unstable when the $E_{\text{form}}^{\text{atom}}(AX)$ is used. On the other hand, 21 compounds listed in Table I can be found to be unstable when the definition of Eq. (1) is adapted.

As shown in Fig. 2, the distribution of $E_{\text{form}}(\text{Cu}X)$ seems to be different from that of $E_{\text{form}}(\text{Ag}X)$ and $E_{\text{form}}(\text{Au}X)$. To understand the dynamical stability relationship among 2D compounds, we plot S for AgX and AuX as a function of CuX in Figs. 3(a) and 3(b), respectively. The trend of the dynamical stability for CuX is not similar to that for AgX and AuX because the plots of S are largely scattered around the dashed lines $S(\text{Cu}X) = S(\text{Ag}X)$ and $S(\text{Cu}X) = S(\text{Au}X)$. In addition, even if CuX in the BHC structure is dynamically stable, i.e., $S(\text{Cu}X) \simeq 1$, AgX and AuX in the BHC structure are unstable, i.e., $S(\text{Ag}X) \ll 1$ or $S(\text{Au}X) \ll 1$, and vice versa: For $X = $ Be, Co, and Ni, CuX is dynamically stable while AgX and AuX are unstable. On the other hand, for $X = $ Mg, Sc, Ti, Zr, Hf, Cr, and Cd, AgX and AuX are dynamically stable while CuX is unstable. These anomalies can be explained by negatively large values of $E_{\text{form}}(AX)$ for $X = $ Be, Co, Ni, Mg, Sc, and Cd: for example, CuBe (-0.42 eV), AgBe (0.35 eV), and AuBe (0.25 eV) (see Table I). An interesting finding is that the value of S for AgX is well correlated with that of AuX, as shown in Fig. 3(c). The correlation coefficient between AgX and AuX is 0.94, whereas that between CuX and AgX (AuX) is 0.49 (0.42). The strong correlation of S between AgX and AuX is attributed to the similar distribution of E_{form} in Fig. 2.

Combined with the correlation of S between AgX and AuX and the stability relationship between 2D and 3D structures, we can predict stable compounds that have not been
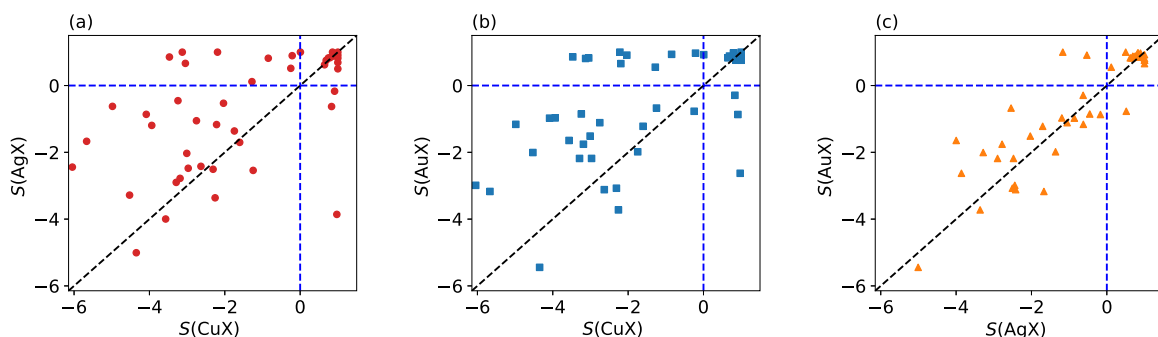

FIG. 3. Relationship of S between AX and BX: (a) $(A, B) = (\text{Cu, Ag})$, (b) $(A, B) = (\text{Cu, Au})$, and (c) $(A, B) = (\text{Ag, Au})$. The diagonal line (dashed) indicates $S(AX) = S(BX)$.
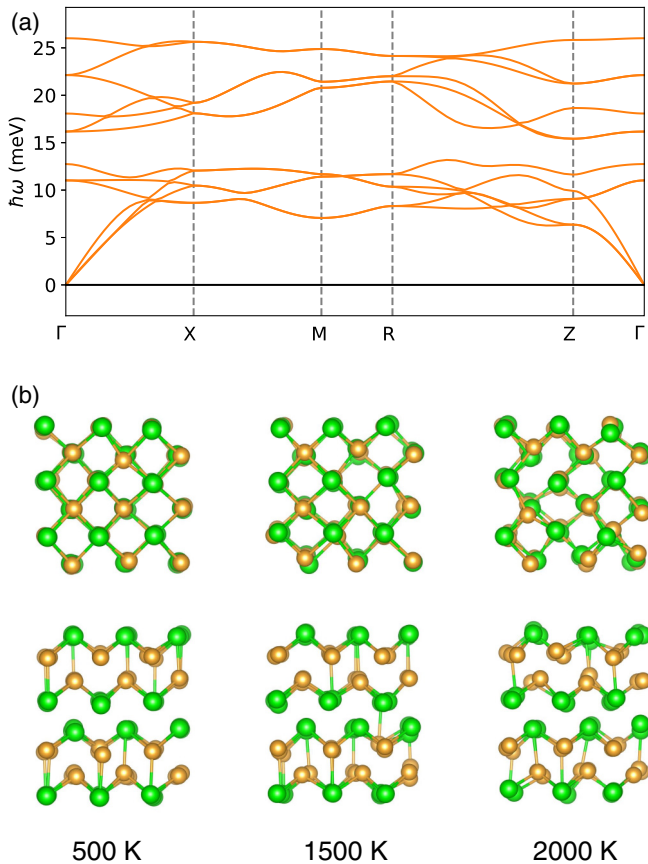
FIG. 5. Plot of $d(A\text{-}A)/d(A\text{-}X)$ vs the column of X in the Periodic Table for the BHC CuX, AgX, and AuX.

AgPd, AgPt, and CuPt listed in Table I are consistent with the prediction by Nelson *et al.* [34], where AgPd, AgPt, and CuPt have the $L1_1$ structure as its ground state. This is because if the BHC structure is dynamically stable, then the $L1_1$ structure is also stable [24]. An implication in this section is that the 2D and 3D structures must be interrelated *via the dynamical stability*.

B. Structure relationship

We next study how the structural parameters of the BHC structure are related to those of the 3D counterparts. To investigate this, we list the values of $d(A\text{-}A)$ and $d(A\text{-}X)$ in Table II. If the value of $d(A\text{-}A)$ is smaller than that of $d(A\text{-}X)$, the coordination number is equal to 6 because of a strong intralayer bonding ($A\text{-}A$ and $X\text{-}X$). In contrast, if an interlayer bonding ($A\text{-}X$) is rather strong, an inequality $d(A\text{-}A)/d(A\text{-}X) > 1$ will hold, leading to a smaller coordination number of 3.

We consider the cases of $X = $ Cu, Ag, and Au, where the inequality of $d(A\text{-}A)/d(A\text{-}X) < 1$ holds. We remind the reader that the noble metals (Cu, Ag, and Au) prefer to have the fcc structure with the largest coordination number of 12. Therefore, the inequality of $d(A\text{-}A)/d(A\text{-}X) < 1$ for the 2D Cu, Ag, and Au in the BHC structure reflects the close-packed structure in the 3D Cu, Ag, and Au. By using the ATOM WORKS database [29], we found that the mixing of noble metals produces a solid solution in the fcc structure represented by $Cu_{0.5}Ag_{0.5}$ [35], $Cu_{0.5}Au_{0.5}$ [36], and $Ag_{0.5}Au_{0.5}$ [37]. These support the high coordination numbers in 2D CuAg, CuAu, and AgAu.

To study the structural trends for the AX in the BHC structure, we plot the values of $d(A\text{-}A)/d(A\text{-}X)$ versus the column of X in the Periodic Table, as shown in Fig. 5. When X is an element of columns 1, 2, 3, and 4, the inequality of $d(A\text{-}A) > d(A\text{-}X)$ holds. [The AX's including alkali metals of K, Rb, and Cs have $d(A\text{-}A)/d(A\text{-}X) = \sqrt{3}$, i.e., no buckling structure.] We remind the reader that noble metals can mix with some elements of columns 1, 2, and 3 to form the B2 structure, such as AuRb and AuCs [38], AgMg [39], AuMg [40], and AgSc and AuSc [41], where the coordination number is 8, which is smaller than 12. We can attribute the inequality of $d(A\text{-}A)/d(A\text{-}X) > 1$ partially to the formation of the B2 structure of AX. When the column of X is from 5 to 10, the magnitude of $d(A\text{-}A)$ is smaller than that of $d(A\text{-}X)$, implying

500 K · 1500 K · 2000 K

FIG. 4. (a) The phonon dispersions of AuZr in the B11 structure and (b) the atomic distribution of the $3 \times 2 \times 2$ supercell after the first-principles MD simulation of 3.2 ps under 500, 1500, and 2000 K. The views are from the c-axis (top) and the a-axis (bottom).

synthesized yet experimentally. Let us consider the cases of $X = $ Ti, Zr, and Hf, where AgX and AuX are dynamically stable as listed in Table I. By using the ATOM WORKS database [29], we found that AgTi [30], AgZr [31], AgHf [32], AuTi [33], and AuHf [33] in the B11 structure have already been synthesized experimentally. We thus identify an anomaly that no synthesis of AuZr in the B11 structure has been reported so far. We then calculated the phonon dispersions of AuZr, as shown in Fig. 4(a). No imaginary phonon frequencies are observed along the symmetry lines. To study the temperature effect on the dynamical stability, we also performed first-principles molecular-dynamics (MD) simulation. The B11 AuZr is stable up to 1500 K, whereas many interatomic bonds are broken at 2000 K [see Fig. 4(b)].

It is quite interesting that the synthesis probability of B11 AuZr has been predicted to be 91.1%, according to the MATERIALNET program [26]. This synthesizability was derived from machine-learning the time evolution of the materials stability network, where the network is constructed from the convex free-energy surface of inorganic materials. In this way, different approaches have predicted the stability of B11 AuZr, so that we expect that AuZr in the B11 structure will be potentially synthesized in future experiments.

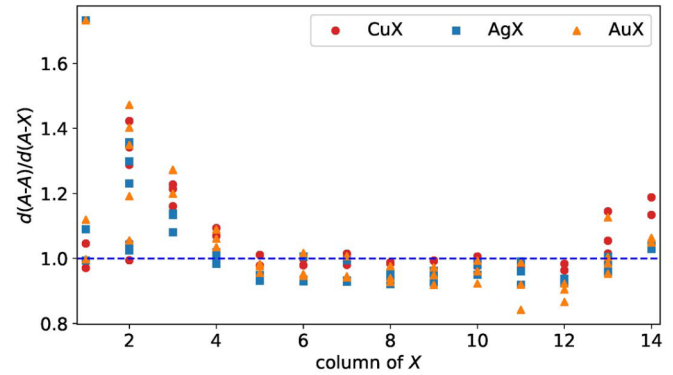By considering the stability relationship between 2D and 3D structures again, the positive values of S for the BHC

a strong intralayer bonding as in the BHC Cu, Ag, and Au (column 11). However, for X = column 12, it is difficult to rationalize the inequality of $d(A\text{-}A) < d(A\text{-}X)$ because AZn (A = Cu [42], Ag [43], and Au [40]), AgCd [44], and AuCd [40] in the B2 structure have been synthesized, as for X = columns 1, 2, and 3. For X = columns 13 and 14 elements, no compounds of the forms of AX and $A_{0.5}X_{0.5}$ have been reported except for X = Al and Ga.

It will be useful to study the trends of the structural parameters of AX with X fixed. Recently, Alsalmi *et al.* studied the stability of CuZn, AgZn, and AuZn in the B2 structure by using DFT [23]. They showed that the bonding strength between the noble metal and the Zn atom becomes stronger as the d orbitals become more extended. In contrast, the core-core repulsion enhances the lattice constant, in turn giving rise to a decrease in the overlap of wave functions. These effects yield nonmonotonic stability properties as one goes from CuZn to AgZn to AuZn, leading to the large lattice parameter of AgZn. In the present calculations, similar behaviors can be observed in the BHC AX: the inequality of $d(\text{Cu-Cu}) < d(\text{Au-Au}) < d(\text{Ag-Ag})$ or $d(\text{Cu-}X) < d(\text{Au-}X) < d(\text{Ag-}X)$ can hold. For the cases of X = Tl, Sn, and Pb, the relationship between $d(\text{Cu-Cu})$, $d(\text{Ag-Ag})$, and $d(\text{Au-Au})$ is quite different.

C. Elastic property

To study the stability of AX against the in-plane deformations, we list the values of c_{11}, c_{12}, c_{22}, and $\log_{10} \Delta$ for the selected AX in Table III. For all cases, the inequality of $\log_{10} \Delta > 0$ holds, indicating that these AX in the BHC structure are elastically stable. For the 2D simple metals (i.e., $A = X$), the elastic constants of the BHC structure are larger than those of the HX structure reported in Ref. [2]: the values of (c_{11}, c_{12}, c_{22}) are (75.4, 25.2, 75.1), (48.9, 18.9, 55.1), and (93.9, 38.9, 92.8) in units of GPa nm for the HX Cu, Ag, and Au, respectively. The enhancement of the elastic constants is due to the finite thickness of the BHC structure. The BHC CuAg, CuAu, and AgAu have the averaged elastic constants of the constituents in the BHC structure (i.e., Cu, Ag, or Au). The AX with X the alkali metal seems to have small values of c_{ij} ($i, j = 1, 2$) and Δ, while the Rh-, Pd-, and Pt-based compounds have relatively large values of c_{ij} and Δ.

The trend of the magnitude of c_{ij} among the same X is that the Ag-based compounds have small values of c_{ij} (see the cases of X = Li, Rh, Pd, Pt, and Ga). This reflects the large value of a_{lat} of AgX that arises from a competition between the core-core repulsion and the d-electron delocalization, which has been studied in Sec. III B. For the cases of X = Ti, Mn, and Al, however, the trend of the c_{ij} is quite anomalous: the AgTi has the largest c_{ij} among ATi; the c_{11} and c_{12} increase monotonically as one goes from CuMn to AgMn to AuMn; and the c_{ii} decreases monotonically while c_{12} increases monotonically as one goes from CuAl to AgAl to AuAl. It is noteworthy that for AgTi, AgMn, and AgAl the intralayer bonding is stronger than the interlayer bonding [i.e., $d(A\text{-}A)/d(A\text{-}X) < 1$], while the opposite tendency [i.e., $d(A\text{-}A)/d(A\text{-}X) > 1$] is observed when the Ag atom is replaced with the Cu or Au atoms in those compounds (see Table II). What is important in this section is that the correlation between the lattice parameters and the elastic constants
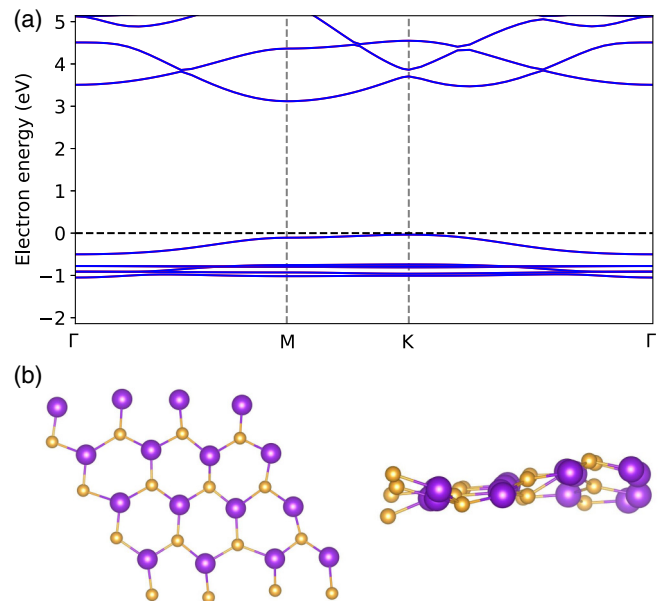

FIG. 6. (a) The electron band structure of AuK in the BHC structure, and (b) the top and side views of the atomic distribution of the $4 \times 4 \times 1$ supercell (32 atoms) after the first-principles MD simulation of 1 ps under 150 K, indicating an instability against out-of-plane vibrations.

depends strongly on the column of X in the Periodic Table. It will be interesting to explore whether similar correlations can be found in other compounds AX (i.e., A is not restricted to noble metals), while such an investigation is beyond the scope of the present work.

D. Electronic and magnetic properties

For practical applications, band-gap engineering of 2D materials has been studied by introducing an electric field, strain, and foreign atoms [45]. It is noteworthy that for 3D compounds, AuRb and AuCs in the B2 structure have been known as semiconductors [46], although both Rb and Cs are metallic elements. Recently, Adeleke *et al.* predicted that at high pressure K_2Ni is a semiconductor with an indirect band gap of 0.65 eV, which is due to a Peierls gap opening [47]. It will be interesting to study which 2D compounds including two metallic elements may exhibit a semiconducting property.

The spin-dependent electron band structure for CuX, AgX, and AuX in the BHC structure is provided in the Supplemental Material [28]. Basically, nearly flat d-bands are located below the Fermi level by a few eV. As in the band structure of elemental metals, the location of d-bands tends to be shallow and deep for CuX and AgX, respectively. The s electron band is modified by mixing with other electrons of X as well as the s-d coupling, and it crosses the Fermi level.

We identify that the compounds with alkali metals X = K, Rb, and Cs are semiconductors. Figure 6(a) show the electron band structure of AuK, showing an indirect semiconductor with a band gap of 3.16 eV, where the valence-band maximum and the conduction-band minimum are located at the K and M points, respectively. Although the DFT within the generalized gradient approximation underestimates the magnitude of the

band gap, the BHC AX (A = Cu,Ag,Au; X = K,Rb,Cs) can be included in one of the wide-gap semiconductors such as hexagonal BN [48] and 2D GaN [49]. Among them, AuK in the BHC structure is predicted to be dynamically stable at zero temperature. However, first-principles MD simulation predicts that it is unstable even at low temperature of 150 K, as shown in Fig. 6(b). While the hexagonal symmetry is almost preserved (top view), the out-of-plane displacement is significantly large (side view) at 1 ps, giving rise to a failure of self-consistent field convergence. The instability against the temperature is due to small phonon energies (a few meV) of the flexural modes around the M and K points (see Fig. S1 in the Supplemental Material [28]).

Note that the long-range Coulomb interactions will be important in the phonon calculations of polar materials. When such an effect is included in the BHC AuX (X = K, Rb, and Cs), the band splitting (a few meV) around the Γ point in the optical phonon branches is observed. The value of S for AuK is reduced to $S = 0.30$. In contrast, the values of S for AuRb and AuCs increase to 0.42 and -0.26, respectively, while imaginary frequencies are still present. It is highly desirable to propose a substrate material for stabilizing these BHC compounds. The phonon dispersions for the BHC AuK, AuRb, and AuCs treated as insulators are provided in the Supplemental Material [28].

We proceed now to the study of the magnetic property. In general, the reduced dimensionality may enhance the magnitude of the magnetic moments [50]. It was recently predicted that 18 elemental metals show a finite magnetic moment in the 2D structures, while there are only five magnetic elements in the 3D structures [6]. Also, the Cu-based compounds in the BHC structure exhibit a relatively high magnetic moment compared to their 3D counterparts [24]. The replacement of Cu with Ag or Au in the 2D compounds will change a bonding character between adjacent atoms and the degree of d electron localization as well, leading to an increase and/or a decrease in the magnetic moment.

Table IV lists the magnetic moment of selected compounds AX in the BHC structure. Even when nonmagnetic elements (X = Sr, Ba, Ti, Zr, Hf, V, Ru, Os, Rh, and Ir) are included, finite magnetic moments appear due to the different profile of electron bands between up and down spins (see the Supplemental Material [28]). This tendency is similar to the DFT calculations for 2D elemental metals [6]. CuX tends to have a smaller magnetic moment than AgX and AuX. The following interpretation will be applied: Among Cu, Ag, and Au, the lattice parameters of CuX are smallest, as listed in Table II and discussed in Sec. III B; the hybridization of the orbital between different atoms will be strong in CuX; and the delocalization of the d electron yields a decrease in the band splitting.

The coupling between the magnetism and the dynamical stability has long been investigated for elemental metals [51]. An interesting feature in the present calculations is that the 2D compounds including antiferromagnetic elements of Cr and Mn have a large magnetic moment about 4 μ_B and are also dynamically stable. On the other hand, the 2D compounds with ferromagnetic elements of Fe, Co, and Ni have finite magnetic moments but are unstable except for CuCo and CuNi. The latter is similar to the tendency observed in our

TABLE IV. The magnetic moment (in units of μ_B per cell) of CuX, AgX, and AuX in the BHC structure. The magnetic moments for the dynamically stable structures ($S \geqslant 0.6$) are shown in bold.

	A		
X	Cu	Ag	Au
Sr	0.17	0.14	0.34
Ba	0.66	0.61	0.65
Ti	0.87	**1.01**	**1.14**
Zr	0.70	**0.64**	**0.82**
Hf	0.75	**0.75**	**0.90**
V	0.02	1.13	0.88
Cr	0.00	**4.29**	**4.28**
Mn	**3.85**	**4.20**	**4.31**
Fe	2.64	3.00	3.09
Ru	0.01	1.19	1.42
Os	0.00	0.01	0.38
Co	**1.74**	1.86	1.95
Rh	**0.59**	**0.82**	**0.98**
Ir	0.01	0.17	0.71
Ni	**0.46**	0.61	0.72

previous calculations [4], where magnetic effects led to an instability of 2D Fe and Co in the buckled square structure.

In our previous work [25], we predicted that the BHC AuTi is unstable against the excitation of phonons at the M and K points by performing spin-unpolarized calculations. In the present work, BHC AuTi has a finite magnetic moment as listed in Table IV and is dynamically stable. The magnetic effect on the dynamical stability of AX seems to depend strongly on the column of X.

IV. SUMMARY

We systematically investigated the dynamical stability, the elastic stability, and the structural property of the BHC CuX, AgX, and AuX, where X is 46 metallic elements in the Periodic Table, by using the first-principles approach. We identified 48 compounds to be dynamically stable by quantifying the profile of the phonon spectra. We demonstrated that the dynamical stability property of AgX is correlated with that of AuX. We predicted that as a 3D compound AuZr in the B11 structure is dynamically stable. This was speculated by a strong correlation of the quantity for the dynamical stability between AgX and AuX. Furthermore, the stability of B11 AuZr is consistent with a high value of the synthesis probability (more than 90%) estimated in Ref. [26]. Future work will explore another interrelationship of structural and dynamical properties between the 2D and 3D compounds through a more comprehensive search in the Periodic Table and/or other structures (including solid solutions) and with use of a machine learning approach.

In addition, we calculated the electronic and magnetic properties of BHC AX. When X = K, Rb, and Cs, the AX was predicted to be a wide-gap semiconductor, while a substrate material is needed to stabilize the out-of-plane vibrations. AgCr, AuCr, CuMn, AgMn, and AuMn were predicted to show a ferromagnetic phase with a large magnetic moment. An interesting but complex relationship between the

magnetism and the dynamical stability was also identified. The investigation of the impact of the different functionals (such as DFT $+ U$ [52]) on these properties of the BHC compounds is left for future work.

APPENDIX: METHODS

We optimized the parameters a_{lat} and δ for the BHC AX and a_{lat} for the HX elemental metals X by using the DFT implemented in the QUANTUM ESPRESSO (QE) package [53]. We used an ultrasoft pseudopotential [54] and an exchange-correlation functional parametrized by Perdew, Burke, and Ernzerhof within the generalized gradient approximation [55]. The self-consistent field (SCF) calculations were performed by setting the energy cutoff to be 80 and 800 Ry for the wave function and the charge density, respectively, and we set the energy convergence to be 10^{-10} Ry. The k grid was assumed to be $30 \times 30 \times 1$ [56] with a smearing parameter of 0.02 Ry [57]. The value of c in a_3 was set to be 14 Å to avoid spurious interactions between different cells along the z axis. The threshold values for geometry optimization were set to be 10^{-5} Ry for the total energy and 10^{-4} a.u. for the total force. Spin-polarized calculations were performed for all compounds, where a ferromagnetic phase was assumed as an initial guess of the SCF calculations. We identified that 13 HX elemental metals of $X =$ Sc, Y, Lu, Cr, Mn, Fe, Ru, Os, Co, Rh, Ir, Ni, and Pd show the ferromagnetic phase. The parameters (the size of the k grid and the threshold values for geometry optimization) used in the present work are equal to those used in the previous work for elemental metals [4].

We next calculated the phonon dispersions of the BHC AX along the symmetry lines of Γ-M-K-Γ by using density-functional perturbation theory (DFPT) [58] implemented in QE. The parameters for the SCF calculations were the same as the geometry optimization calculations above. The convergence parameter for the DFPT calculations was set to be tr2_ph $= 10^{-14}$. The q grid was assumed to be $6 \times 6 \times 1$ (seven q points in the irreducible Brillouin zone). By diagonalizing the dynamical matrix, we finally obtain the phonon frequencies $\omega_\alpha(\boldsymbol{q})$ at the wave vector $\boldsymbol{q}$ in the αth band with $\alpha = 1, \ldots, 6$. If $\omega_\alpha(\boldsymbol{q})$ is imaginary, the BHC structure is unstable against such a phonon mode. When the BHC compounds are treated as insulators, the nonanalytic term accounting for the long-range Coulomb interactions is included to the dynamical matrix.

For the single atom of X, the value of $\varepsilon_{atom}(X)$ was evaluated by using QE [53]. We performed atom-in-a-box calculations of a single atom X in a unit cell with a volume of $15 \times 15 \times 15$ Å^3, where the spin-unpolarized approximation was adapted.

By using QE [53], we optimized the geometry of B11 AuZr with the use of the cutoff energies of 60 and 600 Ry for the wave function and the charge density, respectively, and a $16 \times 16 \times 16$ k grid. The optimized lattice parameters were $a = 3.554$ Å and $c = 6.391$ Å for the tetragonal unit cell. The phonon dispersion calculation was done by assuming a $3 \times 3 \times 3$ q grid. We also performed first-principles MD simulation implemented in QE [53]. We used a $3 \times 3 \times 2$ supercell (72 atoms) by considering the Γ point in the Brillouin zone and set the ionic temperature of 500, 1000, 1500, and 2000 K by using the velocity scaling method. A time step of 20 a.u. (0.96 fs) was adapted, and 3300 MD steps were done, corresponding to 3.2 ps.

To calculate the c_{ij}'s ($i, j = 1, 2$) that are equal to the derivative of the total energy density with respect to the strain ε_x and ε_y, the finite-difference approximation was used by assuming the orthorhombic unit cell including four atoms. The atomic positions were relaxed when the strain along the x and y directions was imposed, where the magnitude of the strain was set to be 0.01. The total energy density was obtained by dividing the total energy per cell by the area of $\sqrt{3}a_{lat}^2$.

[1] G. Zagler, M. Reticcioli, C. Mangler, D. Scheinecker, C. Franchini, and J. Kotakoski, CuAu, a hexagonal two-dimensional metal, 2D Mater. **7**, 045017 (2020).

[2] J. Nevalaita and P. Koskinen, Atlas for the properties of elemental two-dimensional metals, Phys. Rev. B **97**, 035411 (2018).

[3] J. Hwang, Y. J. Oh, J. Kim, M. M. Sung, and K. Cho, Atomically thin transition metal layers: Atomic layer stabilization and metal-semiconductor transition, J. Appl. Phys. **123**, 154301 (2018).

[4] S. Ono, Dynamical stability of two-dimensional metals in the periodic table, Phys. Rev. B **102**, 165424 (2020).

[5] S. Ono, Two-dimensional square lattice polonium stabilized by the spin-orbit coupling, Sci. Rep. **10**, 11810 (2020).

[6] Y. Ren, L. Hu, Y. Shao, Y. Hu, L. Huang, and X. Shi, Magnetism of elemental two-dimensional metals, J. Mater. Chem. C **9**, 4554 (2021).

[7] F. F. Zhu, W. J. Chen, Y. Xu, C. L. Gao, D. D. Guan, C. H. Liu, D. Qian, S. C. Zhang, and J. F. Jia, Epitaxial growth of two-dimensional stanene, Nat. Mater. **14**, 1020 (2015).

[8] F. Reis, G. Li, L. Dudy, M. Bauernfeind, S. Glass, W. Hanke, R. Thomale, J. Schäfer, and R. Claessen, Bismuthene on a SiC substrate: A candidate for a high-temperature quantum spin Hall material, Science **357**, 287 (2017).

[9] V. Kochat, A. Samanta, Y. Zhang, S. Bhowmick, P. Manimunda, S. A. S. Asif, A. S. Stender, R. Vajtai, A. K. Singh, C. S. Tiwary, and P. M. Ajayan, Atomically thin gallium layers from solid-melt exfoliation, Sci. Adv. **4**, e1701373 (2018).

[10] J. Yuhara, B. He, N. Matsunami, M. Nakatake, and G. L. Lay, Graphene's latest cousin: Plumbene epitaxial growth on a "Nano WaterCube," Adv. Mater. **31**, 1901017 (2019).

[11] T. Wang, M. Park, Q. Yu, J. Zhang, and Y. Yang, Stability and synthesis of 2D metals and alloys: A review, Mater. Today Adv. **8**, 100092 (2020).

[12] M. Ashton, J. Paul, S. B. Sinnott, and R. G. Hennig, Topology-Scaling Identification of Layered Solids and Stable Exfoliated 2D Materials, Phys. Rev. Lett. **118**, 106101 (2017).

[13] K. Choudhary, I. Kalish, R. Beams, and F. Tavazza, High-throughput identification and characterization of two-dimensional materials using density functional theory, Sci. Rep. **7**, 5179 (2017).

[14] S. Haastrup, M. Strange, M. Pandey, T. Deilmann, P. S. Schmidt, N. F. Hinsche, M. N. Gjerding, D. Torelli, P. M. Larsen, A. C. Riis-Jensen, J. Gath, K. W. Jacobsen, J. J. Mortensen, T. Olsen, and K. S. Thygesen, The computational 2D materials database: High-throughput modeling and discovery of atomically thin crystals, 2D Mater. **5**, 042002 (2018).

[15] J. Zhou, L. Shen, M. D. Costa, K. A. Persson, S. P. Ong, P. Huck, Y. Lu, X. Ma, Y. Chen, H. Tang, and Y. P. Feng, 2DMat-Pedia, an open computational database of two-dimensional materials from top-down and bottom-up approaches, Sci. Data **6**, 86 (2019).

[16] M. Fukuda, J. Zhang, Y.-T. Lee, and T. Ozaki, A structure map for AB_2 type 2D materials using high-throughput DFT calculations, Mater. Adv. **2**, 4392 (2021).

[17] Z. Lin, L. V. Zhigilei, and V. Celli, Electron-phonon coupling and electron heat capacity of metals under conditions of strong electron-phonon nonequilibrium, Phys. Rev. B **77**, 075133 (2008).

[18] M. Xu, J. Y. Yang, S. Zhang, and L. Liu, Role of electron-phonon coupling in finite-temperature dielectric functions of Au, Ag, and Cu, Phys. Rev. B **96**, 115154 (2017).

[19] M. Bauer, A. Marienfeld, and M. Aeschlimann, Hot electron lifetimes in metals probed by time-resolved two-photon photoemission, Prog. Surf. Sci. **90**, 319 (2015).

[20] A. Giri, J. T. Gaskins, L. Li, Y. S. Wang, O. V. Prezhdo, and P. E. Hopkins, First-principles determination of the ultrahigh electrical and thermal conductivity in free-electron metals via pressure tuning the electron-phonon coupling factor, Phys. Rev. B **99**, 165139 (2019).

[21] D. Pettifor, *Bonding and Structure of Molecules and Solids* (Oxford University Press, New York, 2002).

[22] A. Jain, S. P. Ong, G. Hautier, W. Chen, W. D. Richards, S. Dacek, S. Cholia, D. Gunter, D. Skinner, G. Ceder, and K. A. Persson, The Materials Project: A materials genome approach to accelerating materials innovation, APL Mater. **1**, 011002 (2013).

[23] O. Alsalmi, M. Sanati, R. C. Albers, T. Lookman, and A. Saxena, First-principles study of phase stability of bcc XZn (X = Cu, Ag, and Au) alloys, Phys. Rev. Materials **2**, 113601 (2018).

[24] S. Ono, Metastability relationship between two- and three-dimensional crystal structures: a case study of the Cu-based compounds, Sci. Rep. **11**, 14588 (2021).

[25] S. Ono and H. Satomi, High-throughput computational search for two-dimensional binary compounds: Energetic stability versus synthesizability of three-dimensional counterparts, Phys. Rev. B **103**, L121403 (2021).

[26] M. Aykol, V. I. Hegde, L. Hung, S. Suram, P. Herring, C. Wolverton, and J. S. Hummelshøj, Network analysis of synthesizable materials discovery, Nat Commun. **10**, 2018 (2019).

[27] H. Şahin, S. Cahangirov, M. Topsakal, E. Bekaroglu, E. Akturk, R. T. Senger, and S. Ciraci, Monolayer honeycomb structures of group-IV elements and III-V binary compounds: First-principles calculations, Phys. Rev. B **80**, 155453 (2009).

[28] See Supplemental Material at http://link.aps.org/supplemental/10.1103/PhysRevMaterials.5.104004 for phonon dispersions and spin-dependent electron band structure for AX in the BHC structure.

[29] Y. Xu, M. Yamazaki, and P. Villars, Inorganic materials database for exploring the nature of material, Jpn. J. Appl. Phys. **50**, 11RH02 (2011).

[30] V. N. Eremenko, Yu. I. Buyanov, and N. M. Panchenko, Constitution diagram of the system titanium-silver, Powder Metall. Met. Ceram. **8**, 562 (1969).

[31] Z. Kanghou, Z. Huaizhi, and Z. Yuehua, An investigation of the Ag-Zr phase diagram, J. Less-Common Met. **138**, 173 (1988).

[32] K. Schubert, H. G. Meissner, A. Raman, and W. Rossteutscher, Einige strukturdaten metallischer phasen (9), Naturwissenschaften **51**, 287 (1964).

[33] K. Schubert, H. G. Meissner, and M. Pötzschke, W. Rossteutscher, and E. Stolz, Einige strukturdaten metallischer phasen (7), Naturwissenschaften **49**, 57 (1962).

[34] L. J. Nelson, G. L. W. Hart, and S. Curtarolo, Ground-state characterizations of systems predicted to exhibit $L1_1$ or $L1_3$ crystal structures, Phys. Rev. B **85**, 054203 (2012).

[35] R. K. Linde, Lattice parameters of metastable silver-copper alloys, J. Appl. Phys. **37**, 934 (1966).

[36] T. U. Nahm, K. H. Park, S. J. Oh, S. M. Chung, and G. K. Wertheim, Partial spectral weights of disordered Cu-Au alloys, Phys. Rev. B **52**, 16466 (1995).

[37] Y. C. Venudhar, L. Iyengar, and K. V. K. Rao, Temperature dependence of the lattice parameter and the thermal expansion of Ag-Au (50 at. %) alloy by an X-ray method, J. Less-Common Met. **60**, P41 (1978).

[38] G. A. Tinelli and D. F. Holcomb, NMR and structural properties of CsAu and RbAu, J. Solid State Chem. **25**, 157 (1978).

[39] S. N. Sharma and A. Weiss, Thermal and X-ray investigations of the quasi-binary system $Ag_{1-x}Pd_xMg$ (if $0 \leqslant x \leqslant 0.5$), J. Less-Common Met. **104**, L5 (1984).

[40] Y. Matsuo, S. Minamigawa, and K. Katada, Phase relation of the AuCd-AuMg and AuCd-AuZn quasibinary alloys, Trans. Jpn. Inst. Met. **22**, 367 (1981).

[41] A. T. Aldred, Intermediate phases involving scandium, https://www.osti.gov/servlets/purl/4772375.

[42] S. Shimizu, Y. Murakami, and S. Kachi, Lattice softening and martensitic transformation in Cu-Ni-Zn β phase alloys, J. Phys. Soc. Jpn. **41**, 79 (1976).

[43] H. Iwasaki, T. Fujimura, M. Ichikawa, S. Endo, and M. Wakatsuki, Pressure-induced phase transformation in AgZn, J. Phys. Chem. Solids **46**, 463 (1985).

[44] C. B. Walker and M. Marezio, A single-crystal X-ray study of order in β'-AgCd, J. Appl. Phys. **34**, 1443 (1963).

[45] A. Chaves, J. G. Azadani, H. Alsalman, D. R. da Costa, R. Frisenda, A. J. Chaves, S. H. Song, Y. D. Kim, D. He, and J. Zhou, Bandgap engineering of two-dimensional semiconductor materials, npj 2D Mater. Appl. **4**, 29 (2021).

[46] W. E. Spicer, Photoemission and band structure of the semiconducting compound CsAu, Phys. Rev. **125**, 1297 (1962).

[47] A. A. Adeleke, E. Stavrou, A. O. Adeniyi, B. Wan, H. Gou, and Y. Yao, Two good metals make a semiconductor: A

potassium-nickel compound under pressure, Phys. Rev. B **102**, 134120 (2020).

[48] C. R. Dean, A. F. Young, I. Meric, C. Lee, L. Wang, S. Sorgenfrei, K. Watanabe, T. Taniguchi, P. Kim, K. L. Shepard, and J. Hone, Boron nitride substrates for high-quality graphene electronics, Nat. Nanotechnol. **5**, 722 (2010).

[49] Z. Al Balushi, K. Wang, R. K. Ghosh *et al.*, Two-dimensional gallium nitride realized via graphene encapsulation, Nat. Mater. **15**, 1166 (2016).

[50] C. A. F. Vaz, J. A. C. Bland, and G. Lauhoff, Magnetism in ultrathin film structures, Rep. Prog. Phys. **71**, 056501 (2008).

[51] G. Grimvall, B. Magyari-Köpe, V. Ozoliņš, and K. A. Persson, Lattice instabilities in metallic elements, Rev. Mod. Phys. **84**, 945 (2012).

[52] V. I. Anisimov, F. Aryasetiawan, and A. I. Lichtenstein, First-principles calculations of the electronic structure and spectra of strongly correlated systems: The LDA+U method, J. Phys. Condens. Matter **9**, 767 (1997).

[53] P. Giannozzi, O. Andreussi, T. Brumme, O. Bunau, M. B. Nardelli, M. Calandra, R. Car, C. Cavazzoni, D. Ceresoli, M. Cococcioni *et al.*, Advanced capabilities for materials modeling with Quantum ESPRESSO, J. Phys.: Condens. Matter **29**, 465901 (2017).

[54] A. Dal Corso, Pseudopotentials periodic table: From H to Pu, Comput. Mater. Sci. **95**, 337 (2014).

[55] J. P. Perdew, K. Burke, and M. Ernzerhof, Generalized Gradient Approximation Made Simple, Phys. Rev. Lett. **77**, 3865 (1996).

[56] H. J. Monkhorst and J. D. Pack, Special points for Brillouin-zone integrations, Phys. Rev. B **13**, 5188 (1976).

[57] N. Marzari, D. Vanderbilt, A. De Vita, and M. C. Payne, Thermal Contraction and Disordering of the Al(110) Surface, Phys. Rev. Lett. **82**, 3296 (1999).

[58] S. Baroni, S. Gironcoli, A. Dal Corso, and P. Giannozzi, Phonons and related crystal properties from density-functional perturbation theory, Rev. Mod. Phys. **73**, 515 (2001).